JJ

Sw 9432

ISSN 1340-3745

ICRR-Report-321-94-16
KEK Preprint 94-50
TKU-PAP-94-2
KOBE-AP-94-01
NGTHEP-94-1
OULNS-94-01
TIT-HPE-94-04
GIFU-PH-94-01
INS-Rep.-1035
UPR-0226E

Atmospheric ν_μ / ν_e Ratio in the Multi-GeV Energy Range

KAMIOKANDE Collaboration

(June 1994)

Submitted to Physics Letters B

INSTITUTE FOR COSMIC RAY RESEARCH
UNIVERSITY OF TOKYO
3-2-1 Midori-cho, Tanashi, Tokyo 188, Japan

Atmospheric ν_μ/ν_e Ratio in the Multi-GeV Energy Range

Y.Fukuda, T.Hayakawa, K.Inoue, T.Ishida, S.Joukou, T.Kajita, S.Kasuga,
Y.Koshio, T.Kumita, K.Matsumoto, M.Nakahata, K.Nakamura, A.Sakai,
M.Shiozawa, J.Suzuki, Y.Suzuki and Y.Totsuka
Institute for Cosmic Ray Research, University of Tokyo, Tanashi, Tokyo 188, Japan

K.S.Hirata, K.Kihara, M.Mori[1], Y.Oyama, A.Suzuki[2], and M.Yamada [3]
National Laboratory for High Energy Physics (KEK), Tsukuba, Ibaraki 305, Japan

M.Koshiba and K.Nishijima
Tokai University, Shibuya, Tokyo 151, Japan

T.Kajimura[4], T.Suda[5] and A.T.Suzuki
Department of Physics, Kobe University, Kobe, Hyogo 657, Japan

T.Ishizuka, M.Koga[2], K.Miyano, H.Miyata, H.Okazawa, and H.Takei[6]
Niigata University, Niigata, Niigata 950-21, Japan

T.Hara, N.Kishi, Y.Nagashima, M.Takita and A.Yoshimoto[7]
Department of Physics, Osaka University, Toyonaka, Osaka 560, Japan

[1]Present address: Department of Physics, Miyagi University of Education, Sendai, Miyagi 980, Japan

[2]Present address: Faculty of Science, Tohoku University, Sendai, Miyagi 980, Japan

[3]Present address: Niigata Polytechnic College, Niigata 957, Japan

[4]Present address: Hydrographic Department, Maritime Safety Agency, Chuo-ku, Tokyo 104, Japan

[5]Deceased

[6]Present address: Oarai Engeneering Center, Power Reactor & Nuclear Fuel Department Corporation, Oarai, Ibaraki, 311-13, Japan

[7]Present address: Public System Development Division, NEC Corporation, Minato-ku, Tokyo 105, Japan

Y.Hayato, K.Kaneyuki, Y.Takeuchi and T.Tanimori
Department of Physics, Tokyo Institute of Technology, Meguro, Tokyo 152, Japan

S.Tasaka
Department of Physics, Gifu University, Gifu, Gifu 501-11, Japan

K.Nishikawa
Institute for Nuclear Study, University of Tokyo, Tanashi, Tokyo 188, Japan

E.W.Beier, E.D.Frank, W.Frati, S.B.Kim [8], A.K.Mann, F.M.Newcomer,
R.Van Berg and W.Zhang [9]
Department of Physics, University of Pennsylvania, Philadelphia PA 19104, U.S.A.

Abstract

Data from the Kamiokande detector were used to study the atmospheric $(\nu_\mu + \overline{\nu}_\mu)/(\nu_e + \overline{\nu}_e)$ ratio in the multi-GeV energy range. The observed ratio of μ-like to e-like events relative to the calculated ratio, $(\mu/\mathrm{e})_{data}/(\mu/\mathrm{e})_{MC} = 0.57\ ^{+0.08}_{-0.07}\ \pm 0.07$, suggests that the atmospheric $(\nu_\mu + \overline{\nu}_\mu)/(\nu_e + \overline{\nu}_e)$ ratio is smaller than expected for these neutrino energies. Also studied was the zenith-angle dependence of the above ratio. Results of an analysis of neutrino oscillations are presented.

[8]Present address: University of Michigan, Ann Arbor, MI48109, U.S.A.

[9]Present address: NASA/Goddard Space Flight Center, Greenbelt, MD 20771, U.S.A.

It is understood that sensitive studies of neutrino oscillations are possible by measuring the atmospheric $(\nu_\mu + \overline{\nu}_\mu)/(\nu_e + \overline{\nu}_e)$ ratio. In recent years, considerable work has been devoted to measure this ratio. Kamiokande [1], IMB-3 [2] and Soudan-2(preliminary) [3] observed that the μ/e ratio of atmospheric neutrino interactions with energies of about 1 GeV (or less) was significantly smaller than expected, suggesting that the atmospheric $(\nu_\mu+\overline{\nu}_\mu)/(\nu_e+\overline{\nu}_e)$ ratio is smaller than expected. A detailed analysis of the data based on the assumption of neutrino oscillations indicated that the allowed regions in the oscillation parameter space from the Kamiokande data were; $\Delta m^2 > 4\times10^{-3}eV^2$ and $\sin^2 2\theta > 0.3$ for $\nu_\mu \leftrightarrow \nu_e$ oscillations, and $\Delta m^2 > 1\times10^{-3}eV^2$ and $\sin^2 2\theta > 0.4$ for $\nu_\mu \leftrightarrow \nu_\tau$ oscillations [1]. Also, it was pointed out that the data might be explained by proton decays into $e^+\nu\nu$[4]. In this paper, we extended the study of the μ/e ratio from atmospheric neutrino interactions into the multi-GeV energy region.

The Kamiokande-II-III (Kam-II-III) detector is a 4.5-kton water Cerenkov detector located at a depth of 2700 meters water equivalent in the Kamioka mine in Japan. It consists of two layers of water, each instrumented with two dimensional arrays of 50 cm diameter photomultiplier tubes (PMTs) covering all surfaces. The inner volume of water constitutes an inner-detector, which detects Cerenkov photons radiated by relativistic charged particles produced by atmospheric neutrino interactions. The outer layer surrounds the inner-detector constituting a 4π solid-angle anti-counter. The anti-counter is useful for identifying entering cosmic-ray muons and measuring any leakage of energy of the atmospheric-neutrino interactions occurring in the inner-detector. Pulse-height and timing information from each PMT are recorded and used in the data analysis. For more details of the detector, see, for example, Ref.[5] for Kam-II and Ref.[6] for Kam-III.

In the previous analysis of the Kamiokande data, fully-contained events with visible-energy (E_{vis}) less than 1.33 GeV were used. E_{vis} is defined to be proportional to the number of observed photoelectrons (p.e.), and equal, within the energy resolution of the detector, to the primary energy for electrons and gammas. For muons, E_{vis} is smaller than the primary momentum: E_{vis} =1.33 GeV corresponds to 1.5 GeV/c for muons. Here we present the data from atmospheric-neutrino interactions in the multi-GeV energy range in the Kam-II-III detector. These are (i) fully-contained events with E_{vis} larger than 1.33 GeV, and (ii) partially-contained events which have their interaction vertex in the

fiducial volume and at least one visible track exiting from the inner-detector. These data constitute a completely independent data sample from the already published one, i.e., there is no overlap of events between these two samples. Hereafter, we call this sample the 'multi-GeV' data to distinguish it from the already published 'sub-GeV' data.

These multi-GeV data are useful from two points of view. First, the ratio of the number of μ-like to e-like events normalized by the corresponding ratio of the Monte Carlo (MC) simulation ($(\mu/e)_{data}/(\mu/e)_{MC}$) provides an independent measurement of that ratio to be compared with the result from the sub-GeV data. Second, valuable information on neutrino oscillations might be extracted by studying the zenith-angle dependence of the μ/e ratio. This is made possible by the large difference of the path-length between downward-going neutrinos ($\lesssim$20 km) and upward-going neutrinos ($\approx10^4$ km), together with the better angular correlation between the neutrinos and the produced charged-leptons for these multi-GeV neutrinos (r.m.s.=15$\sim$20°) relative to the angular correlation (r.m.s.$\sim$60°) in the sub-GeV range.

The selection criteria for fully-contained events with E_{vis} higher than 1.33 GeV are: (1) $E_{vis} > 1.33$ GeV, (2) (total p.e. numbers of the anti-counter) < 20, or (total hit PMTs of the anti-counter) ≤ 5, and (3) the vertex position of the event should be at least 1 m inside the PMT plane. The fiducial volume for these events is 1.35 kton. We observed 195 such fully contained events during 8.2 kton·yr of the Kam-II-III detector exposure. Of them, all single ring events are subject to particle identification. Then each event is classified as either e- or μ-like. In a multi-ring event, the lepton flavor can be identified if the charged lepton carries a significant fraction of the total visible energy. Thus we use some fraction (about 30%) of the multi-ring events for the study of the μ/e ratio. A Cerenkov ring that contributes more than 80% of the total visible energy is assumed to be due to a lepton and the particle identification is applied to the ring. This procedure successfully selects charged current(CC) ν_e and CCν_μ events. We observed 31 (21 single-ring and 10 multi-ring) such μ-like and 98 (73 single-ring and 25 multi-ring) such e-like events. According to the Monte Carlo events, the purity of CCν_μ and CCν_e in the selected μ-like and e-like events are greater than 95% and 90%, respectively.

The selection criteria for the partially-contained events were described in Ref.[12]. Here we give only an outline of the selection criteria. They are; (1)(total p.e. numbers

of the inner counter) > 1500 (1200 for about 30% of the data), (2)elimination of entering tracks by calculating the probability that a track is a cosmic-ray muon, (3) at most one cluster of hit PMTs in the anti-counter, (4) (total p.e. numbers of the anti-counter) > 20, and (total hit PMTs of the anti-counter) > 5, (5) the reconstructed vertex position should be at least 1.5 m inside the PMT plane. The fiducial volume for these events is 1.04 kton. The detection efficiency of the partially-contained events in the fiducial volume is estimated to be 92% by MC events. We observed 118 such partially-contained events during 6.0 kton·yr of the Kam-II-III detector exposure. Muons that have energy higher than a few GeV cannot be contained in the Kamiokande detector. Accordingly, the partially-contained events are dominated by multi-GeV CC ν_μ interactions. However, there are non-negligible contaminations of CC ν_e and NC events. We make a simple cut to improve the purity of CC ν_μ events in the partially-contained μ-like sample. A single-ring partially-contained event is eliminated if it is identified as e-like, which eliminates about 8% of the partially-contained events. All the multi-ring partially-contained events are taken to be μ-like. 94% of the remaining partially-contained events are estimated to be due to CC ν_μ interactions, and we assign all these events as μ-like. (We do not use the single-ring partially-contained e-like events in the analysis, because the estimated fraction of CC ν_e in this category of events is only 42%.) We observed 104 such partially-contained μ-like events.

Fig. 1 shows the vertex position and the direction distribution for the observed fully-contained e- and μ-like events and partially-contained μ-like events. One sees no evidence for the contamination of cosmic-ray muons, i.e., no evidence for the excess of downward- and inward-going events at the top and side boundaries of the fiducial volume. We estimate that the contamination of non-neutrino origin in these data is less than 1%.

To understand these events quantitatively, Monte Carlo simulated events [7] are generated and passed through the same analysis procedure as the data. In this analysis two fluxes are used. One is the flux calculated in Ref.[8] (Flux A). The other is the flux of Ref.[9] for neutrino energy (E_ν) <3 GeV and Ref.[10] for E_ν >10 GeV. For E_ν between 3 and 10 GeV the two fluxes are smoothly connected (Flux B). These calculated fluxes are suitable for the present study, because the flux values for ν_e, $\overline{\nu}_e$, ν_μ and $\overline{\nu}_\mu$ from (lower than) 100 MeV to (higher than) 100 GeV are available, and the muon-polarization effect

and the geomagnetic cutoff are taken into account. Table 1 summarizes the data and compares them with the corresponding Monte Carlo simulations, which are seen to be in good agreement with each other.

Figs. 2(a) ~ (c) show the E_{vis} distributions which are informative for understanding the energy range relevant to the present study. Although some of the partially-contained μ-like events appear in the E_{vis} distribution in Fig. 2(c) below 1 GeV, as is predicted by the Monte Carlo simulation, the energy of neutrinos giving rise to these are as shown in Fig. 2(f). Based on the Monte Carlo simulations shown in Figs. 2(d) ~ (f), the mean energy of neutrinos is 5 GeV for the fully-contained e-like events, 2.5 GeV for the fully-contained μ-like events, and 9 GeV for the partially-contained μ-like events. If we combine the fully-contained μ-like and partially-contained μ-like events, the mean energy of neutrinos for these μ-like events is 7 GeV. Thus the mean neutrino energies are similar for μ-like and e-like events in these samples. These numbers suggest that the μ/e ratio can be obtained by combining the multi-GeV fully-contained and partially-contained events, i.e., $\mu/e \equiv$ (fully-contained μ-like + partially-contained μ-like events)/(fully-contained e-like events). From Table 1, one can calculate:

$$\frac{(\mu/e)_{data}}{(\mu/e)_{MC}} = 0.57^{+0.08}_{-0.07}(\text{stat.}) \pm 0.07(\text{syst.}) \qquad \text{(based on Flux A)},$$

which suggests that the atmospheric $(\nu_\mu + \overline{\nu}_\mu)/(\nu_e + \overline{\nu}_e)$ ratio is smaller than expected for the multi-GeV energy range. This result agrees well with that obtained in the sub-GeV data[1]. (See also a description below for an updated sub-GeV result.) This observation further suggests that proton decays into $e^+\nu\nu$[4] are not the (main) cause of the small μ/e ratio.

We turn now to the systematic error involved in the μ/e ratio. The uncertainty in the $(\nu_\mu + \overline{\nu}_\mu)/(\nu_e + \overline{\nu}_e)$ ratio in the energy range of a few GeV to a few tens of GeV is estimated to be about 5% based on a comparison of the two fluxes, A and B. To test the sensitivity to the atmospheric $\overline{\nu}/\nu$ ratio, we took an error of 10% in either the $\overline{\nu}_e/\nu_e$ or $\overline{\nu}_\mu/\nu_\mu$, and found a 1% change in the μ/e ratio. For the neutrino energies relevant to the present study, the masses of the charged leptons (electrons and muons) are much smaller

than the center of mass energy of the neutrino interactions. Thus the ratio of the CC cross sections of $\nu_\mu(\overline{\nu}_\mu)$ and $\nu_e(\overline{\nu}_e)$ is expected to be almost unity, and the error associated with this ratio is taken to be less than 2%. In the selected e-like and μ-like events, it is estimated that the contaminations of neutral current (NC) events are 5 and 2%, respectively. NC processes producing π^0 in the final state constitute the dominant source of contamination in the e-like events, but a $\pm$50% error in the NC π^0 production changes the μ/e ratio by 3%.

In the data analysis, there are several sources of systematic error. The reduction procedure of the partially-contained events relies on a non-trivial program and depends on calibration constants of the data. Thus a change in calibration constants might change the detection efficiency. The detection efficiency and its uncertainty for events within the fiducial volume is 92$\pm$3%. Since the partially-contained events dominate the μ-like events, this $\pm$3% is adopted as a source of systematic error on the μ/e ratio. The μ/e identification error is smaller in this energy range than in the sub-GeV energy range, and is estimated to be less than 2%. Since it affects the numerator and the denominator in the μ/e ratio in opposite directions, the error due to the μ/e identification in the μ/e ratio is taken as 4%. In the present analysis, multi-ring events with one Cerenkov ring contributing more than 80% of the total E_{vis} are used. The use of such multi-ring events could introduce some biases in the μ/e ratio, if the Monte Carlo did not reproduce the data in some kinematical details. Thus the distribution of (maximum E_{vis} per Cerenkov ring)/(total E_{vis}) was compared between the data and the Monte Carlo, and indicated no sizable difference. The possible error on μ/e due to the use of such multi-ring events is less than 3%. There are other sources of error: 1% from a 5% uncertainty in the absolute energy calibration of the inner-counter; 3% from a 30% uncertainty in the absolute energy calibration, plus 50% uncertainty in the energy resolution of the anti-counter; 3% from the vertex reconstruction; and less than 1% from a background contamination of non-neutrino origin. The statistical error of the Monte Carlo events (6%) is also included in the systematic error. Adding all these errors in quadrature, the systematic error of $(\mu/e)_{data}/(\mu/e)_{MC}$ is estimated to be $\pm$12%. Finally, it should be mentioned that possible errors due to nuclear effects relevant to low-energy neutrino interactions [11] have negligible contribution to the systematic error in the energy range of the present study.

Fig. 3 shows the zenith-angle distribution for the (a) e-like events, and (b) all μ-like events. One sees that the e-like events have a small excess of events for the upward- and horizontal-going directions and the μ-like events have a small deficit of events in the same directions. These non-uniform zenith-angle dependences can more clearly be seen in Fig. 4, which shows the zenith-angle dependence of $(\mu/e)_{data}/(\mu/e)_{MC}$. It should be noted that the systematic error associated with any up/down asymmetry is negligible compared with the statistical error.

A possible explanation of the small $(\mu/e)_{data}/(\mu/e)_{MC}$ and its zenith-angle dependence may be sought in neutrino oscillations. We analyzed the data in terms of two neutrino-oscillation channels, $\nu_\mu \leftrightarrow \nu_e$ and $\nu_\mu \leftrightarrow \nu_\tau$. The method of analysis was similar to that for sub-GeV atmospheric neutrinos[1].

To test for neutrino oscillations, the fully-contained e- and μ-like (FCe and FCμ) events are respectively mapped on (zenith angle(cosΘ), and log(E_{vis})) planes, where (cosΘ, log(E_{vis})) is meshed into (5$\times$8) cells. The range of E_{vis} is from 1.0 to 100 GeV. Similarly, the partially-contained μ-like events (PCμ) are plotted on a cosΘ axis, where cosΘ is divided into 5-bins. Here we do not use the information of E_{vis} for the partially-contained μ-like events, because E_{vis} is not a good measure of the neutrino energy for the partially-contained events. Then a χ^2 is defined to draw contours of allowed regions on the (Δm^2, $\sin^2 2\theta$) plane:

$$\chi^2 = Min.(\alpha,\beta)\left(L(\alpha,\beta) + \frac{\alpha^2}{\sigma_\alpha^2} + \frac{\beta^2}{\sigma_\beta^2}\right),$$

$$\begin{aligned} L(\alpha,\beta) = -2 \times \sum_i \sum_j \Bigg(& ln\left\{\frac{(X_{ij}(FCe))^{N_{ij}(FCe)} \cdot exp(-X_{ij}(FCe))}{N_{ij}(FCe)!}\right\} \\ & + ln\left\{\frac{(X_{ij}(FC\mu))^{N_{ij}(FC\mu)} \cdot exp(-X_{ij}(FC\mu))}{N_{ij}(FC\mu)!}\right\} \\ & + ln\left\{\frac{(X_i(PC\mu))^{N_i(PC\mu)} \cdot exp(-X_i(PC\mu))}{N_i(PC\mu)!}\right\}\Bigg), \end{aligned}$$

$$\begin{aligned} X_{ij}(FCe) &= (1+\alpha)(1-\beta/2)M_{ij}(FCe), \\ X_{ij}(FC\mu) &= (1+\alpha)(1+\beta/2)M_{ij}(FC\mu), \\ X_i(PC\mu) &= (1+\alpha)(1+\beta/2)M_i(PC\mu), \end{aligned}$$

where $N_{i(j)}(FCe,\ FC\mu\ or\ PC\mu)$ is the number of observed fully-contained e- or μ- or partially-contained μ-events in the (cosΘ(i), log(E_{vis}(j))) cell, $M_{i(j)}(FCe,\ FC\mu\ or\ PC\mu)$ is that of a Monte Carlo sample with given oscillation parameters, α is a factor relevant to the absolute normalization with its (systematic) error σ_α=30%, and β to the μ/e ratio with its (systematic) error σ_β=12%. In calculating $M_{i(j)}(FCe,\ FC\mu\ or\ PC\mu)$ for $\nu_\mu \leftrightarrow \nu_e$ oscillations, the matter effect is taken into account. A set of (α, β) which minimizes the above χ^2 is calculated for each oscillation parameter set. Then the 90% C.L. allowed regions are calculated. Because the optimum value of $\sin^2 2\theta$ lies at its physical bound, the confidence level contours are determined using the prescription for bounded physical regions given in Ref.[13].

The constraints on the oscillation parameters are shown in Fig. 5 where the crosses indicate the best-fit parameters, (Δm^2, $\sin^2 2\theta$) = (1.8×10^{-2}eV^2, 1.0) for $\nu_\mu \leftrightarrow \nu_e$ and (1.6×10^{-2}eV^2, 1.0) for $\nu_\mu \leftrightarrow \nu_\tau$, and the regions inside the thick curves give the 90%C.L. allowed regions. The χ^2 values for these best-fit parameter sets are 172.2 and 176.9 for the $\nu_\mu \leftrightarrow \nu_e$ and $\nu_\mu \leftrightarrow \nu_\tau$ oscillations, respectively.[10] Based on a Monte Carlo study, the mean of the corresponding χ^2 are 173.4 and 173.6 for the $\nu_\mu \leftrightarrow \nu_e$ and $\nu_\mu \leftrightarrow \nu_\tau$ oscillations, respectively. For the MC prediction we used Flux A [8], although no significant difference occurs if Flux B is used. Also shown in Fig. 5 are the constraints on neutrino oscillation parameters based on updated sub-GeV data (see below).

From Fig. 5, one may make the following observations. First, the allowed regions as derived from the sub- and multi-GeV data largely overlap. There is no inconsistency between the sub- and multi-GeV data when interpreting them in terms of neutrino oscillations. Second, the high Δm^2 regions ($\Delta m^2 > 9\times10^{-2}$eV^2 for both the $\nu_\mu \leftrightarrow \nu_e$ and $\nu_\mu \leftrightarrow \nu_\tau$ oscillations) are excluded at 90% C.L. by the present analysis of the multi-GeV data. This is a consequence of the observed zenith-angle dependence.

Since the sub- and multi-GeV data are mutually consistent, we obtained an allowed region of neutrino oscillation parameters based on all the Kamiokande data. The result is also shown in Fig. 5.

The observed zenith-angle dependence of $(\mu/e)_{data}/(\mu/e)_{MC}$ was shown in Fig. 4.

[10]The present definition of χ^2 does not give any direct estimate of the goodness of the fit.

Also shown in Fig. 4 are expectations from the MC simulations for parameter sets (Δm^2, $\sin^2 2\theta$) corresponding to the best fit values for the $\nu_\mu \leftrightarrow \nu_e$ and $\nu_\mu \leftrightarrow \nu_\tau$ oscillations. One sees that the MC predictions which include neutrino oscillations reproduce the data in Fig. 4, and that the observed zenith-angle distribution is consistent with an oscillation interpretation.

To confirm that the obtained results do not depend strongly on the specific choice of the flux calculation or the MC modeling, we repeated the above analysis with σ_α = 100% and σ_β = 100%, i.e., the parameter regions of neutrino oscillations were obtained without relying on the absolute flux calculation and the calculated μ/e ratio. We found that null neutrino-oscillation was excluded at 99% C.L. even in this very conservative assumption. We repeat that this result is a consequence of the observed zenith-angle dependence of $(\mu/e)_{data}/(\mu/e)_{MC}$ in Fig. 4, which supports the neutrino oscillation interpretation independent of the small μ/e ratio.

We compare the results from the present data with those from the sub-GeV data [1] which are fully-contained events with E_{vis} less than 1.33 GeV. The sub-GeV data are updated in Table 2. The systematic error on the sub-GeV μ/e ratio has been discussed in Ref. [1]. The updated value of $(\mu/e)_{data}/(\mu/e)_{MC}$ is $0.60\ ^{+0.06}_{-0.05}$(stat) $\pm$0.05(syst) based on Flux A. This value agrees with that of the multi-GeV data, $0.57\ ^{+0.08}_{-0.07}\ \pm0.07$.

Fig. 6(a) shows the zenith-angle dependence of $(\mu/e)_{data}/(\mu/e)_{MC}$ for the sub-GeV data. The expected zenith-angle dependences for two sets of neutrino oscillation parameters are also shown in the same figure. Since the zenith-angle distributions are quite different between the sub- and multi-GeV data, it is natural to question if these two distributions are physically consistent or not. Especially, it might be informative to show the zenith-angle distribution of the $(\mu/e)_{data}/(\mu/e)_{MC}$ with different momentum cuts for the sub-GeV data. Figs. 6(b) and (c) show the zenith-angle distributions of the $(\mu/e)_{data}/(\mu/e)_{MC}$ with such cuts. The expected zenith-angle distributions for oscillation parameters are also shown. From these figures and Fig. 4 we see that the zenith-angle distributions of the multi- and sub-GeV data are mutually consistent when the data are interpreted as due to neutrino oscillations.

Analyses similar to that described above are possible for the data from other underground experiments. The IMB-3 experiment observed $(\mu/e)_{data}/(\mu/e)_{MC} = 0.54 \pm 0.05(\text{stat}) \pm 0.12(\text{syst.})$ (P_{lepton} <1.5GeV/c)[2], which agrees well with the Kamiokande sub-GeV data. However, the energy range of the published IMB-3 data (P_{lepton} <1.5GeV/c) is not relevant to the present multi-GeV data. The Frejus experiment [14] was the first to systematically study the partially-contained events. During 1.56 kton·yr of the exposure, Frejus found for a data sample with visible-energy greater than 1 GeV, $(\mu/e)_{data}/(\mu/e)_{MC}(> 1\text{GeV})_{\text{Frejus}} = 1.13^{+0.32}_{-0.25}(\text{stat})$, different from the result obtained here at the 2σ level. Published data on upward through-going muons produced in the rock near underground detectors and neutrino oscillation parameters obtained from them [15], [16] are discussed in Ref. [17] (see also [15]), which suggests that the excluded parameter regions from upward-going muon data may be changed substantially by future improvements in the very high energy neutrino flux and cross section calculations.

In summary, we studied the atmospheric $(\nu_\mu + \overline{\nu}_\mu)/(\nu_e + \overline{\nu}_e)$ ratio in the multi-GeV energy range. The μ/e ratio of the data relative to the corresponding ratio from a Monte Carlo simulation was $0.57^{+0.08}_{-0.07}(\text{stat}) \pm 0.07(\text{syst})$ averaging over the complete zenith-angle. We also observed that this ratio showed zenith-angle dependence, unlike the isotropic dependence observed in the sub-GeV data. The data were analyzed assuming neutrino oscillations and yielded allowed regions of the oscillation parameters for both the $\nu_\mu \leftrightarrow \nu_e$ and $\nu_\mu \leftrightarrow \nu_\tau$ channels, consistent with those obtained from our sub-GeV data.

We gratefully acknowledge the cooperation of the Kamioka Mining and Smelting Company. This work was supported by the Japanese Ministry of Education, Science and Culture. Part of the analysis was carried out at the computer facility of the Institute for Nuclear Study, University of Tokyo.

References

[1] K.S.Hirata et al., Phys. Lett. B 205 (1988) 416; Phys. Lett. B 280 (1992) 146.

[2] D.Casper et al., Phys. Rev. Lett. 66 (1991) 2561; R. Becker-Szendy et al., Phys. Rev. D. 46 (1992) 3720.

[3] P.Litchfield, for the Soudan 2 Collaboration, Proc. of the International Workshop on ν_μ/ν_e Problem in Atmospheric Neutrinos, Laboratori Nazionali del Gran Sasso, Italy, March 1993, p114: M.C.Goodman, for the Soudan 2 Collaboration, talk presented at the 23rd International Cosmic Ray Conference, Calgary, Canada, July 1993.

[4] W.A.Mann, T.Kafka, W.Leeson, Phys. Lett. B 291 (1992) 200.

[5] K.S.Hirata et al., Phys. Rev. D 44 (1991) 2241; Phys. Rev. D 45 (1992) 2170(E).

[6] K.Inoue, Dr. Thesis, University of Tokyo, Dec. 1993.

[7] M.Nakahata et al., J. Phys. Soc. Jpn., 55 (1986) 3786.

[8] M.Honda, K.Kasahara, K.Hidaka and S.Midorikawa, Phys. Lett. B 248 (1990) 193; M.Honda, private communication.

[9] G.Barr, T.K.Gaisser and T.Stanev, Phys. Rev. D 39 (1989) 3532.

[10] L.V.Volkova, Sov. J. Nucl. Phys. 31 (1980) 784.

[11] D.D.Koetke et al., Phys. Rev. D 46 (1992) 2554; R.G.H.Robertson, in Proc. of the XXVI International Conference on High Energy Physics, August 1992, Dallas, USA, ed. J.R.Sanford, p140; A.K.Mann, Phys. Rev. D 48 (1993) 422.

[12] N.Sato et al., Phys Rev. D 44 (1991) 2220.

[13] Particle properties data booklet, Section "Gaussian errors – bounded physical region", June 1992.

[14] Ch. Berger et al., Phys. Lett. B 227 (1989) 489.

[15] Y.Oyama et al., Phys. Rev. D 39 (1989) 1481.

[16] R. Becker-Szendy et al., Phys. Rev. Lett. 69 (1992) 1010.

[17] W.Frati, T.K.Gaisser, A.K.Mann and T.Stanev, Phys. Rev. D 48 (1993) 1140.

[18] Ch. Berger et al., Phys. Lett. B 245 (1990) 305.

[19] K.Gabathuler et al., Phys. Lett. B 138 (1984) 449.

[20] F.Dydak et al., Phys. Lett. B 134 (1984) 281.

[21] F.Bergsma et al., Phys. Lett. B 142 (1984) 103.

Table 1. Summary of the multi-GeV data from Kam-II-III and simulated atmospheric neutrino interactions for two fluxes.

	Data(*)	νMC(**)	
		Flux A	Flux B
Fully-contained (E_{vis} > 1.33 GeV)			
Total	195	181.0	189.1
e-like	98(73+25)(***)	66.5(45.9+20.7)	70.8(49.1+21.6)
μ-like	31(21+10)	37.8(25.8+12.0)	40.4(27.3+13.2)
Partially-contained(****)			
Total	118	135.5	136.6
e-like	–	–	–
μ-like	104	124.4	125.4
Total			
e-like	98	66.5	70.8
μ-like	135	162.2	165.8
$(\mu/e)_{data}/(\mu/e)_{MC}$		$0.57^{+0.08}_{-0.07}$	$0.59^{+0.08}_{-0.07}$

*) The detector exposures are 8.2 kton·yr and 6.0 kton·yr for the fully contained and partially contained events, respectively.

**) Each Monte Carlo prediction is based on 51 kton·yr and 40 kton·yr equivalent simulated data for fully-contained and partially-contained events, respectively. The Monte Carlo events are passed through the same analysis chain as the data.

***) Single and multi-ring events.

****) No E_{vis} cut at 1.33 GeV.

Table 2. Summary of the sub-GeV atmospheric neutrino data from Kam-I-II-III. The detector exposure is 7.7 kton·yr.

Type of ev.	Data		νMC(*)			
			Flux A		Flux B	
	total ev.	$\mu \rightarrow$e	total ev.	$\mu \rightarrow$e	total ev.	$\mu \rightarrow$e
Single ring(**)	482	182	584.3	270.5	653.2	301.0
μ-like	234	158	356.8	247.9	396.0	275.6
e-like	248	24	227.6	22.6	257.2	25.4
Multi ring	208	82	233.8	94.1	253.8	101.2
Total ev.	690	264	818.1	364.6	907.0	402.2
$(\mu/e)_{data}/(\mu/e)_{MC}$			$0.60^{+0.06}_{-0.05}$		$0.61^{+0.06}_{-0.05}$	

*) Each Monte Carlo prediction is based on 43kt·yr equivalent simulated data. The Monte Carlo events are passed through the same analysis chain.

**) $0.1< p_e <1.33$ GeV/c for the e-like events and $0.2< p_\mu <1.5$ GeV/c for the μ-like events.

Figure captions

Fig. 1 Two dimensional plots showing vertex position and direction of momentum for the (a) fully-contained events and (b) partially-contained events of the data in the $R^2 - Z$ plane, where R represents the horizontal axis and Z the vertical axis of the cylindrical fiducial volume. The black circles show the vertex positions for the e-like and the white circles those for the μ-like events. The lines associated with the circles show the momentum directions in the $R^2 - Z$ plane. Downward-going particles have the downward-going lines extending from the bottom of the circles. Events with relatively short lines have the momentum directions perpendicular to the $R^2 - Z$ plane.

Fig. 2 Visible-energy (E_{vis}) distributions for the (a) fully-contained e-like events, (b) fully-contained μ-like events and (c) partially-contained μ-like events. The circles with error bars show the data and the histogram the MC (without neutrino oscillations). Monte Carlo predicted neutrino-energy distributions for the (d) fully-contained e-like events, (e) fully-contained μ-like events and (f) partially-contained μ-like events.

Fig. 3 Zenith-angle distributions for the (a) e-like events and (b) μ-like events (the fully-contained and partially-contained events are combined). The circles with error bars show the data and the histogram the MC (without neutrino oscillations). The downward direction is given by $\cos\Theta = 1$.

Fig. 4 Zenith-angle distribution of $(\mu/e)_{data}/(\mu/e)_{MC}$, where both the fully-contained and the partially-contained events are included. The circles with error bars show the data. Also shown are the expectations from the MC simulations with neutrino oscillations for parameter sets (Δm^2, $\sin^2 2\theta$) corresponding to the best-fit values to the multi-GeV data for $\nu_\mu \leftrightarrow \nu_e$ ($(1.8\times10^{-2}\mathrm{eV}^2, 1.0)$, dashes) and $\nu_\mu \leftrightarrow \nu_\tau$ ($(1.6\times10^{-2}\mathrm{eV}^2, 1.0)$, dots) oscillations.

Fig. 5 90% C.L. allowed neutrino-oscillation parameters as obtained from the multi-GeV data (thick curves). 90% C.L. allowed regions as obtained from the updated sub-GeV data are also shown by thick-dotted curves. The allowed regions as obtained by combining the sub- and multi-GeV data are also shown (shaded region). The best-fit values are also shown by dash-crosses (sub-GeV data), full-crosses (multi-GeV data) and stars (sub- and

multi-GeV data combined). The 90% C.L. excluded regions from the other experiments are also shown [15], [16], [18], [19], [20], [21].

Fig. 6 Zenith-angle dependence of $(\mu/e)_{data}/(\mu/e)_{MC}$ for (a) the full sub-GeV data and the sub-GeV data with the minimum momentum cuts at (b) 500 MeV/c and (c) 900 MeV/c. The MC predictions with neutrino oscillations $((\Delta m^2_{\nu_\mu\nu_e}, \sin^2 2\theta_{\nu_\mu\nu_e}) = (2.2\times10^{-2}\mathrm{eV}^2,$ 0.75) (dash, the best-fit parameter set for the sub-GeV data) and $(\Delta m^2_{\nu_\mu\nu_e}, \sin^2 2\theta_{\nu_\mu\nu_e})$ $= (1.6\times10^{-2}\mathrm{eV}^2,$ 0.98) (dash-dot, the best-fit parameter set for all the Kamiokande data) are shown by histograms.

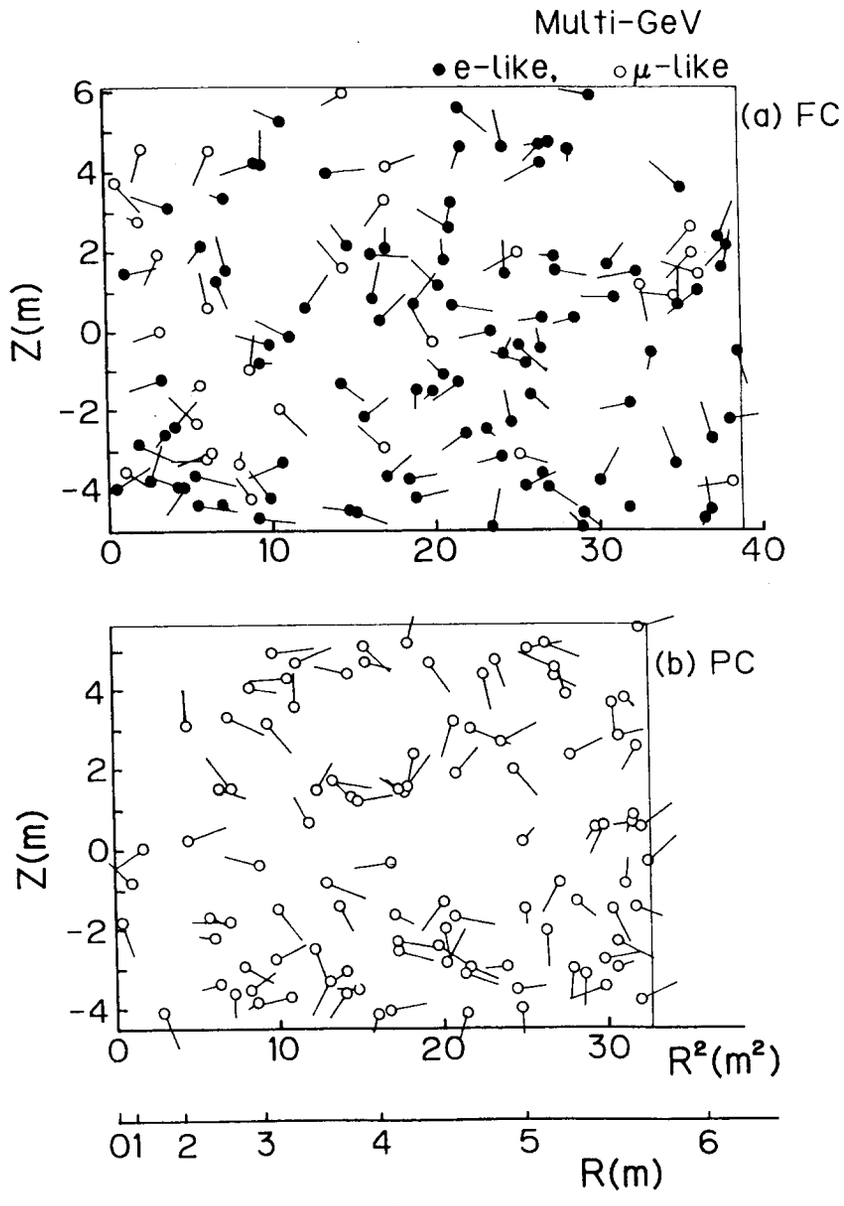

Fig.1

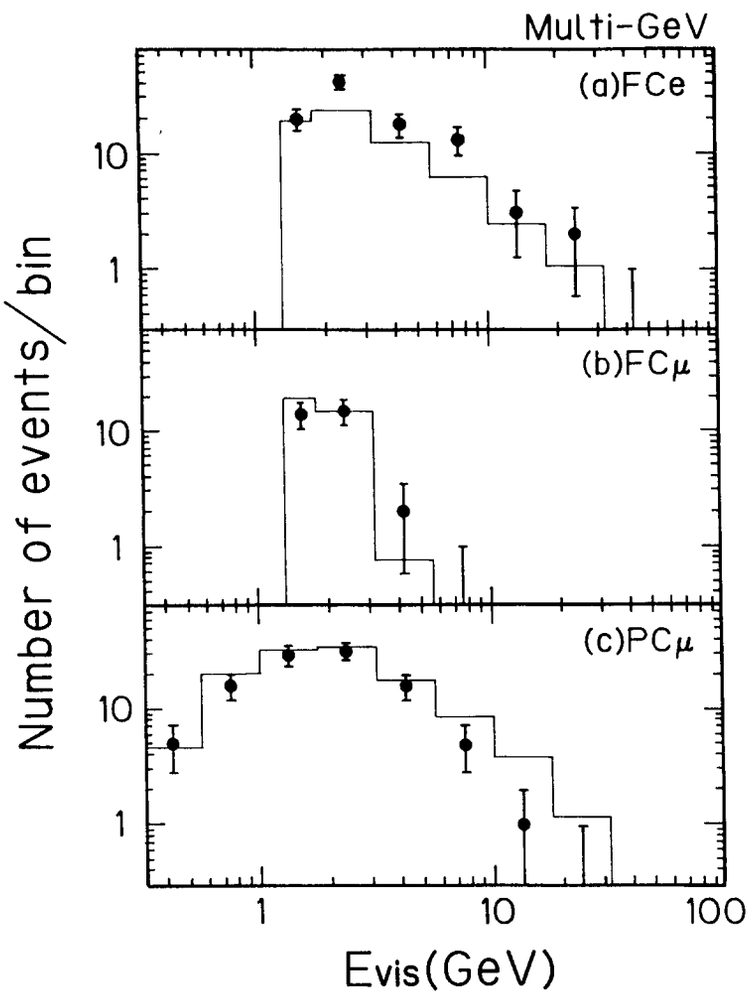
Multi-GeV
(a)FCe
(b)FCμ
(c)PCμ
Number of events/bin
Evis(GeV)
10
1
100

Fig.2

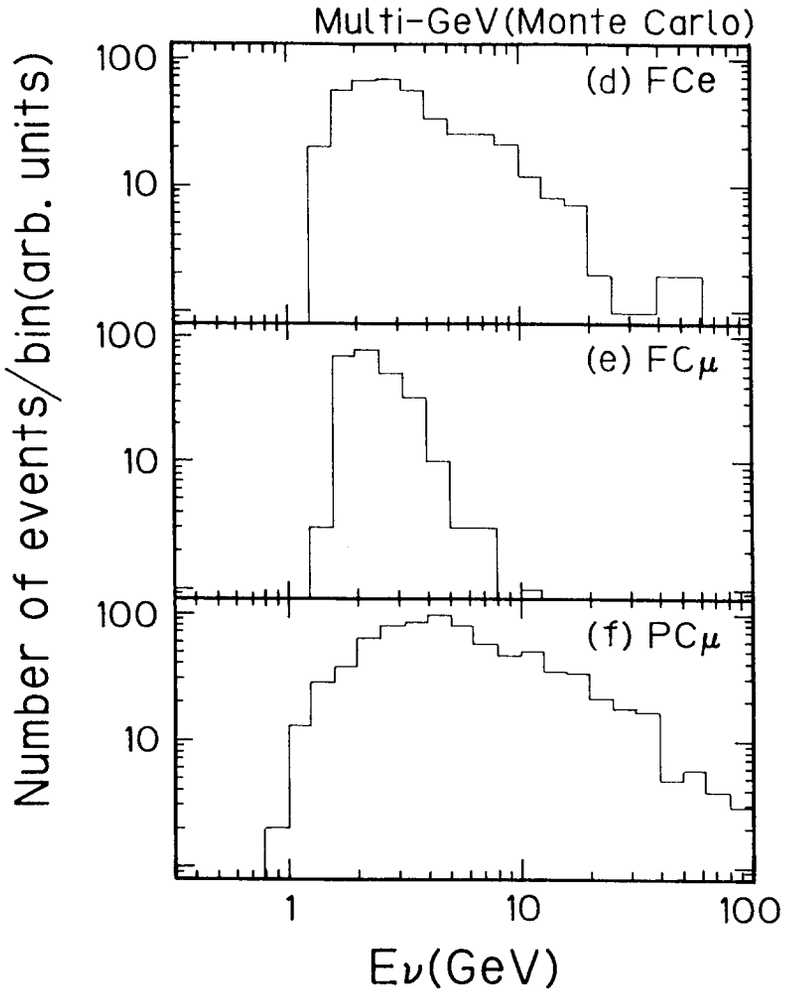
Multi-GeV(Monte Carlo)
(d) FCe
(e) FCμ
(f) PCμ
Number of events/bin(arb. units)
Eν(GeV)
100
10
1

Fig.2

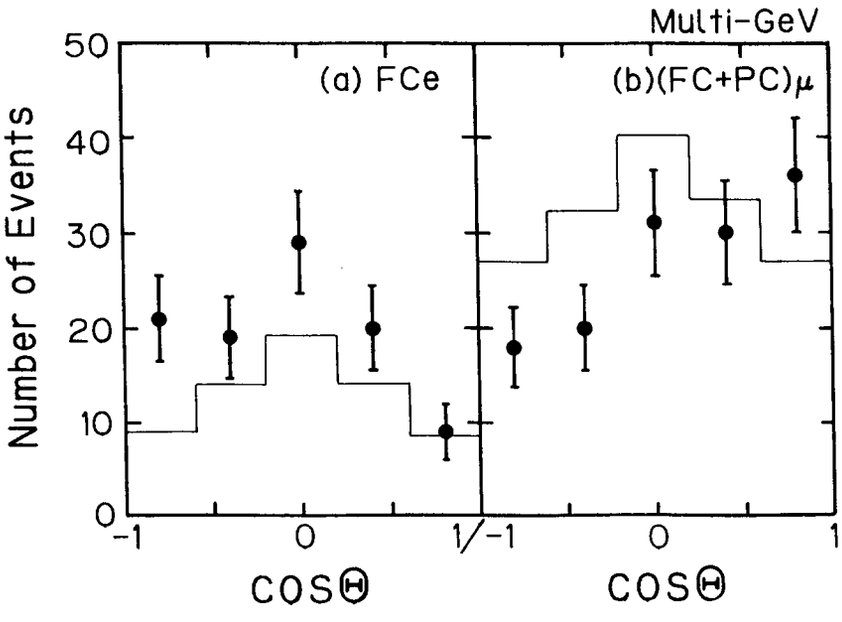
Multi-GeV
(a) FCe
(b)(FC+PC)μ
Number of Events
50
40
30
20
10
0
-1
0
1/-1
0
1
cosΘ
cosΘ

Fig.3

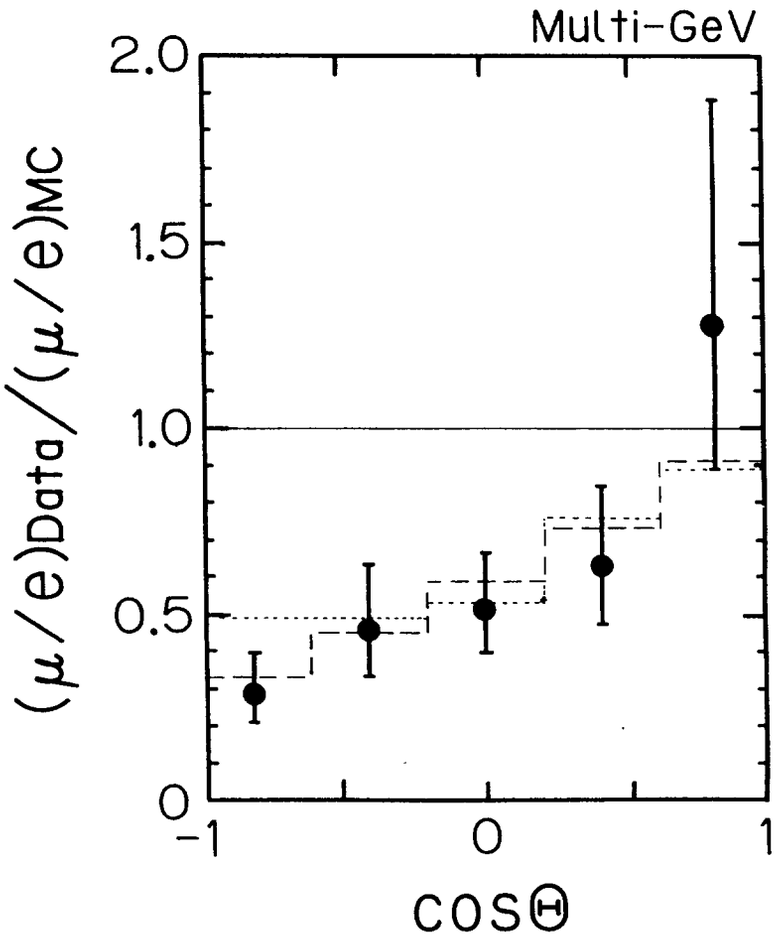
Multi-GeV
(μ/e)Data/(μ/e)MC
2.0
1.5
1.0
0.5
0
-1
0
1
cosΘ

Fig.4

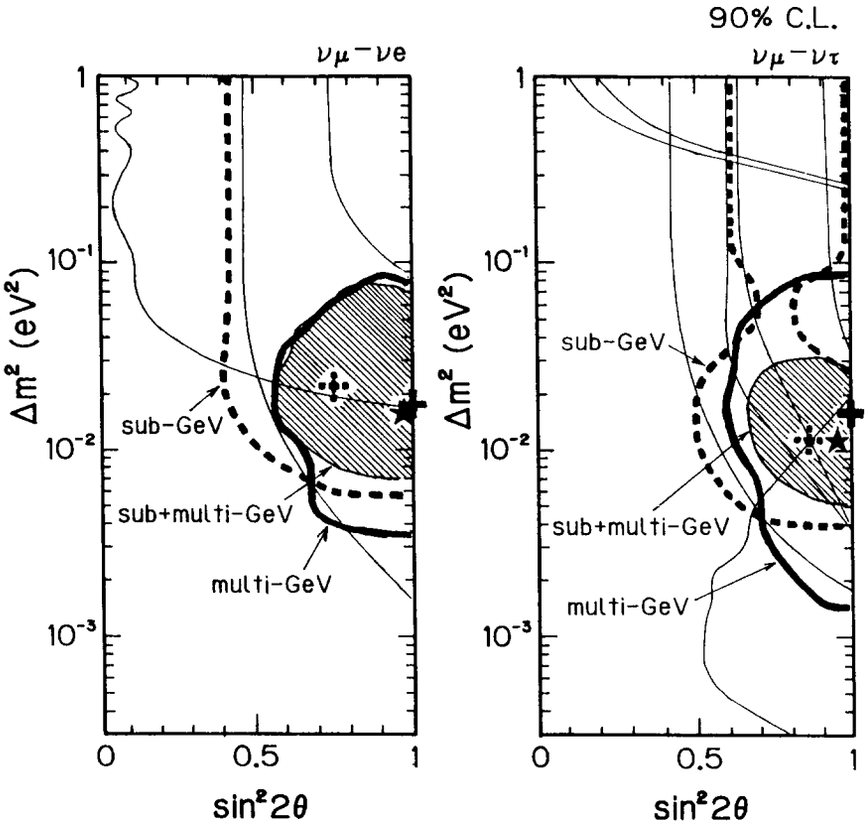
90% C.L.
νμ−νe
νμ−ντ
Δm² (eV²)
sin²2θ
sub-GeV
sub+multi-GeV
multi-GeV

Fig.5

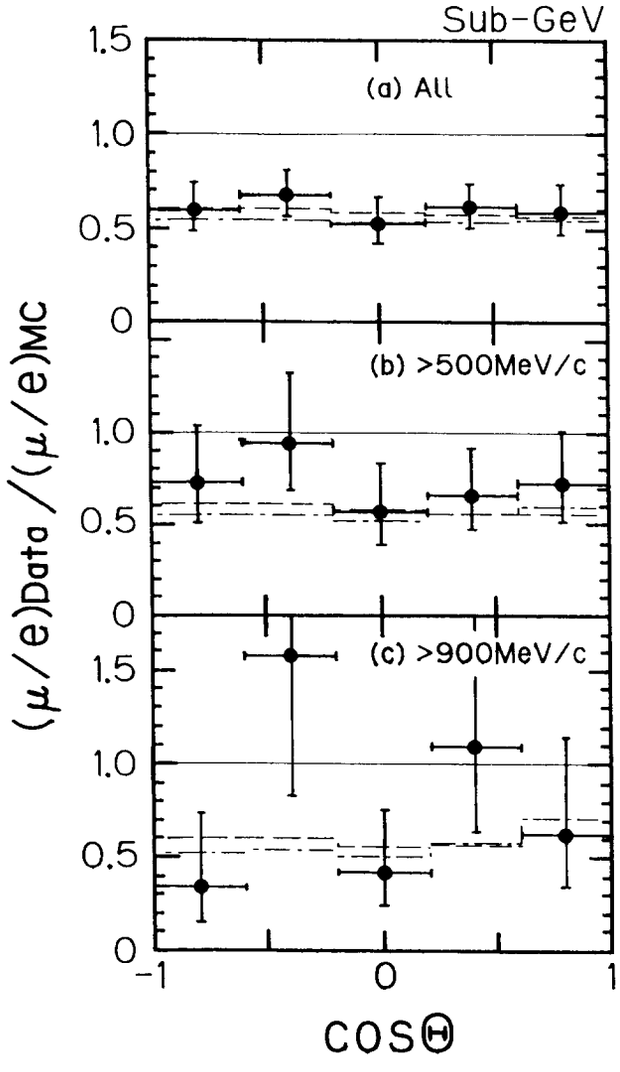
Sub-GeV
(a) All
(b) >500MeV/c
(c) >900MeV/c
(μ/e)Data /(μ/e)MC
COSΘ

Fig.6